

The Rotational Spectra, Isotopically Independent Parameters, and Interatomic Potentials for the $X_1^2\Pi_{3/2}$ and $X_2^2\Pi_{1/2}$ States of BrO

Brian J. Drouin,^{*,1} Charles E. Miller,[†] Holger S. P. Müller,^{*,2} and Edward A. Cohen*

^{*}Jet Propulsion Laboratory, California Institute of Technology, Pasadena, California 91109-8099; and [†]Department of Chemistry, Haverford College, Haverford, Pennsylvania 19041-1392

Received July 27, 2000; in revised form September 25, 2000

Observations of the rotational spectrum of BrO have been extended to include vibrational levels up to $v = 8$ in the $X_1^2\Pi_{3/2}$ and $v = 7$ in the $X_2^2\Pi_{1/2}$ states. The rotational spectra of isotopically enriched Br¹⁸O, X_1 , $v = 0, 1$ and X_2 , $v = 0$ have been observed as well. The spectra of all four isotopic species have been fit to a Hamiltonian in which the parameters have fixed isotopic ratios. An extensive set of isotopically independent parameters has been determined. Interatomic potentials have been derived for both the X_1 and X_2 states. The hyperfine constants and their vibrational dependencies have been determined more precisely and several of them have been determined for the first time. These are interpreted in terms of the electronic structure of the molecule. The isotope relations among the constants have provided a means of decorrelating the electron spin–rotation constant γ from the fine–structure centrifugal distortion constant, A_D , and have allowed the first determination of an effective value for γ . © 2001 Academic Press

INTRODUCTION

The importance of halogen monoxides (XO) in atmospheric chemistry has been extensively documented, especially the participation of XO species in catalytic ozone destruction cycles (1). Recent spectroscopic studies of ClO, BrO, and IO have been driven largely by the need for accurate remote sensing measurements of these molecules in the atmosphere. However, the molecular constants obtained from high-resolution XO spectra also provide detailed electronic structure information that may be correlated with chemical reactivity or used as a benchmark for *ab initio* calculations (2, 3).

As is the case for all the halogen monoxides, BrO has a single vacancy in a $p\pi$ antibonding orbital. This gives rise to an inverted doublet Π ground electronic state. The flame emission spectrum of the A–X system was first observed by Vaidya (4) and later by Coleman and Gaydon (5), who proposed a numbering scheme for the emission bands. High-resolution absorption spectra of BrO were first recorded by Durie and Ramsay for the $A_1^2\Pi_{3/2}$ – $X_1^2\Pi_{3/2}$ electronic transition in the near UV (6). A later study by Barnett *et al.* (7) on ⁸¹BrO revised the vibrational numbering and provided additional rovibrational characterization of both the ground and excited electronic states. Loewenschuss *et al.* (8) had independently suggested the revised numbering based on an analysis of the

matrix isolation spectrum. Recent measurements of the A–X spectrum with Fourier transform spectroscopy (9) and cavity ringdown spectroscopy (10) have confirmed that the predissociation linewidths limit the effective resolution of the spectrum to 1 cm^{-1} .

The BrO ground electronic state has been characterized in considerably greater detail. Gas-phase ESR spectra (11–14) and pure rotational spectra (15–17) have been reported for the $X_1^2\Pi_{3/2}$ state. McKellar (18) observed several low J transitions of the $X_2^2\Pi_{1/2}$ – $X_1^2\Pi_{3/2}$, 0–0 band using LMR spectroscopy and provided a direct measurement of the fine-structure interval, A_0 , as well as well as rotational, Λ -doubling and some hyperfine constants for the X_2 , $v = 0$ state. The fundamental vibrational frequency of the X_1 state has been obtained from rotationally resolved infrared spectra (19, 20). Tamassia and Brown (21) have observed the LMR spectrum of the X_1 , $v = 2$ –0 band. Until now, Ref. (18) and a photoelectron detachment experiment (22) have been the only observations of the X_2 state. An extensive summary of BrO spectroscopy prior to 1996 can be found in a review article by Chase (23).

Recent experiments in this laboratory have resulted in observations of the rotational spectra of vibrationally excited IO radicals in both their $X_1^2\Pi_{3/2}$ and $X_2^2\Pi_{1/2}$ states with internal energies to more than 8000 cm^{-1} or 40% of the I–O bond dissociation energy (24). Methods similar to those used in the IO experiments were found to produce BrO radicals in both the $X_1^2\Pi_{3/2}$ and $X_2^2\Pi_{1/2}$ states with internal energies up to 6700 cm^{-1} . This study extends measurements of the pure rotational spectrum of the BrO X_1 state to include vibrational levels up to $v = 8$ and reports the first pure rotational spectra of the X_2 state, including vibrational levels up to $v = 7$. In addition

Supplementary data for this article are available on IDEAL (<http://www.idealibrary.com>) and as part of the Ohio State University Molecular Spectroscopy Archives (http://msa.lib.ohio-state.edu/jmsa_hp.htm).

¹ Caltech Postdoctoral Scholar at JPL.

² NASA-NRC Resident Research Associate 1995–1997. Present address: I. Physikalisches Institut, Universität zu Köln, Zùlpicher Str. 77, D-50937, Köln, Germany.

rotational spectra of isotopically enriched Br^{18}O , X_1 , $v = 0$, 1 and X_2 , $v = 0$ have been observed. The molecular Hamiltonian used in the analysis follows the work of Brown *et al.* (25), so that the molecular parameters have well-defined mass and/or nuclear moment dependencies. The spectra of the four isotopic species, $^{79,81}\text{Br}^{16,18}\text{O}$, have been fitted with a single set of isotopically independent spectroscopic constants. Parameters describing the deviation of the rotational constant from the Born–Oppenheimer approximation (26) and the effective electron spin–rotation constant, γ , have been determined for the first time. Interatomic potentials, equilibrium bond lengths, and vibrational intervals have been determined for both the X_1 and X_2 states. The vibrational intervals are in good agreement with experiment for the X_1 state (7, 19–21) and provide predictions of the as yet unobserved vibrational spectrum of the X_2 state. The refined spectroscopic parameters have also improved the accuracy of calculations of the submillimeter and far-infrared rotational spectrum. The rotational spectra of the ground and first excited vibrational states have been placed in the JPL *Submillimeter, Millimeter, and Microwave Spectral Line Catalog* (27), which is available online at <http://spec.jpl.nasa.gov>.

EXPERIMENTAL

The spectrometer used in this work has been described in detail previously (28–30). Measurements were carried out in a 1-m-length, 7.3-cm-diameter, temperature-controlled glass cell. A Zeeman coil is wrapped around the entire length of the cell. The vacuum pump which was used is an ordinary rotary vane pump with a maximum throughput of 24 l/s. Spectra were observed at room temperature in selected regions between 62 and 650 GHz. Transitions could be readily assigned on the basis of their distinctive hyperfine patterns as well as their proximity to positions predicted on the basis of earlier work.

Bromine monoxide was produced by two methods. The first was similar to that described in Ref. (17). O atoms were generated by a microwave discharge through O_2 and mixed with Br_2 in the sample cell. BrO production was optimized by monitoring a strong spectral feature while adjusting the gas pressures. Similar results were obtained by adding Br_2 directly to the discharge. In general, O_2 pressures were in the vicinity of 90 mTorr with no more than ≈ 5 mTorr Br_2 . Pressures were reduced to about 20 mTorr O_2 when necessary for improved resolution. All pressures were measured at the exit of the cell under flow conditions using a Baratron pressure sensor. Insofar as could be determined, the BrO produced using an external microwave discharge was in thermal equilibrium with the walls of the cell. This is shown in Fig. 1, where a weak $\Delta F = 0$ doublet of the X_1 state and a group of transitions from the X_2 state are compared with a simulation at 300 K. Under similar conditions iodine monoxide is formed by a chemiluminescent reaction which produces nonthermal distributions of excited states.

Excited states of BrO were generated in a dc discharge along

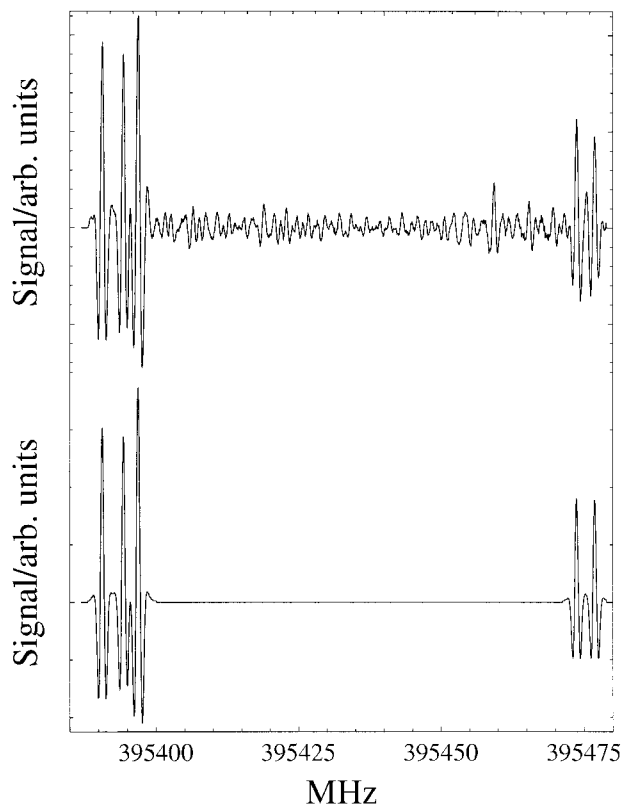


FIG. 1. A single survey scan and 300 K simulation of the ^{79}BrO X_2 , $J = 31/2-29/2$, $\Delta F = 1$ transitions (left) and the ^{81}BrO X_1 , $J = 31/2-29/2$, $F = 14-14$ doublet (right) showing near thermal equilibrium between the X_1 and X_2 states.

the length of the sample cell. The cathode was a 10-cm-wide hollow electrode made of stainless steel shim stock that conformed to the inside diameter of the sample cell. The main valve to the vacuum pump in a sidearm at the opposite end of the cell served as the grounded anode. Approximately 5 mTorr Br_2 and 70 mTorr O_2 were introduced through separate ports near the cathode. Typical discharge conditions were maintained at approximately 1300 V and 40 mA. The cell was kept near room temperature by passing methanol through its cooling jacket. The discharge caused some broadening of the X_1 state rotational transitions due to their nearly first-order Stark effect. This resulted in the blending of closely spaced Λ -doublets whose components are shifted slightly toward each other in a weak electric field. An example of the blending is shown in Fig. 2, where the $v = 2$, $J = 33/2-31/2$ transitions are shown for BrO generated by the two methods just described. Also apparent in the figure is the increase in signal-to-noise ratio (S/N) for excited state in the discharge since the trace for the thermally populated BrO is the average of 13 scans compared to two for BrO in the discharge. Although the excitation is less in BrO than IO, the high excitation of both fine-structure levels in the dc discharge is common to both molecules.

Weaker transitions, i.e., those with $v > 4$ or $\Delta F = 0$, were

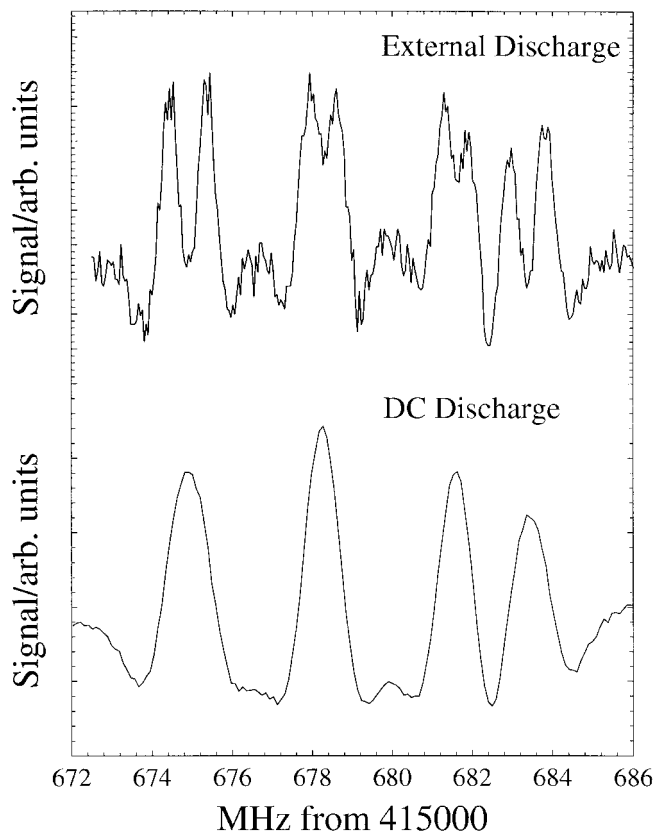


FIG. 2. Comparison of X_1 , $v = 2$, $J = 33/2-31/2$ transitions of BrO generated using an external microwave discharge (top) and an in-cell dc discharge.

averaged over 8–10 scans to improve the S/N. Relative intensities of the rotational transitions for the X_1 , $v + 1$ and X_2 , v states were similar since $E(X_2, v) - E(X_1, v + 1) \approx 240 \text{ cm}^{-1}$. This is shown in Fig. 3 for $v = 3$. A monotonic decrease of relative intensity for increasing energy of the lower states

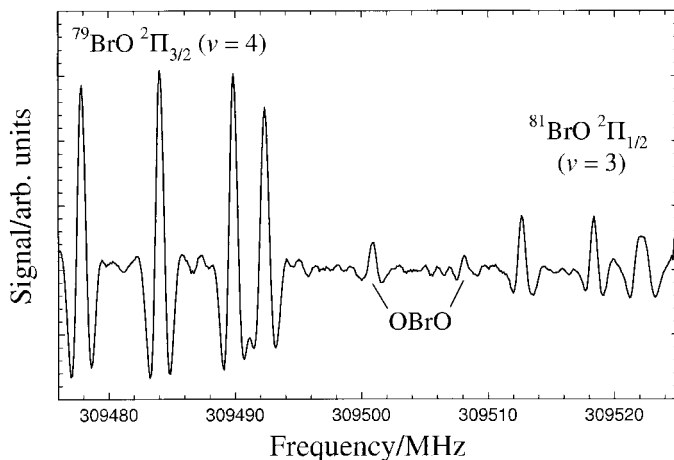


FIG. 3. Comparison of $v = 3$, X_2 and $v = 4$, X_1 transitions observed in a dc discharge.

TABLE 1
 J 's and v 's Included in the Data Set^a

v	Ω	J'
Br ¹⁶ O		
0	3/2	5/2 - 9/2, 19/2, 23/2, 31/2, 33/2, 39/2 - 43/2, 49/2, (51/2)
	1/2	5/2, 7/2, 15/2, 17/2, 25/2, 31/2, 33/2, 41/2
1	3/2	5/2 - 9/2, 25/2, 31/2, 33/2, <u>41/2</u> , 49/2
	1/2	25/2, 33/2
2	3/2	25/2, 33/2
	1/2	(25/2), 33/2
3	3/2	25/2, 33/2
	1/2	25/2, 33/2
4	3/2	25/2, 33/2
	1/2	25/2, 33/2
5	3/2	25/2, 33/2
	1/2	25/2, 33/2, <u>35/2</u>
6	3/2	25/2, 33/2, 35/2
	1/2	35/2
7	3/2	25/2, <u>33/2</u> , 35/2
	1/2	35/2
8	3/2	35/2
Br ¹⁸ O		
0	3/2	27/2, 35/2, 37/2
	1/2	27/2, 35/2, 37/2
1	3/2	27/2, 35/2, 37/2

^a All J 's were observed for both Br isotopes except for those in parentheses or underlined which were observed for only ⁸¹BrO or ⁷⁹BrO, respectively.

was observed. Transitions arising from states higher in energy than X_1 , $v = 8$ and X_2 , $v = 7$ were searched for, but no reasonable assignments could be made due to low S/N and overlap with the numerous OBrO features which were observed ubiquitously throughout the scanning. The OBrO transitions were all easily identified following the work of Müller *et al.* (30). It was found that excess Br₂ could be used to titrate away most of the OBrO without significant change in BrO signal. A magnetic field was sometimes applied to shift OBrO lines with strong Zeeman effect away from BrO X_2 features, all of which have weak Zeeman effect. However, residual OBrO caused significant interference with the weakest BrO features. Transitions of BrO measured in a large magnetic field and those showing blending of hyperfine components are weighted less in the data analysis. Table 1 shows the J 's and v 's of the rotational transitions observed in this study as well as several transitions from our earlier paper (17) which have been included in the fit. In all, 731 features in the rotational spectrum have been fitted with an rms of 37 kHz. These include 451 single lines, 277 unresolved pairs of lines, and two groups of three unresolved lines.

DATA ANALYSIS

The data included in the analysis consist of the rotational data obtained in this study, some measurements from our earlier study of the X_1 state, high-resolution infrared data of the

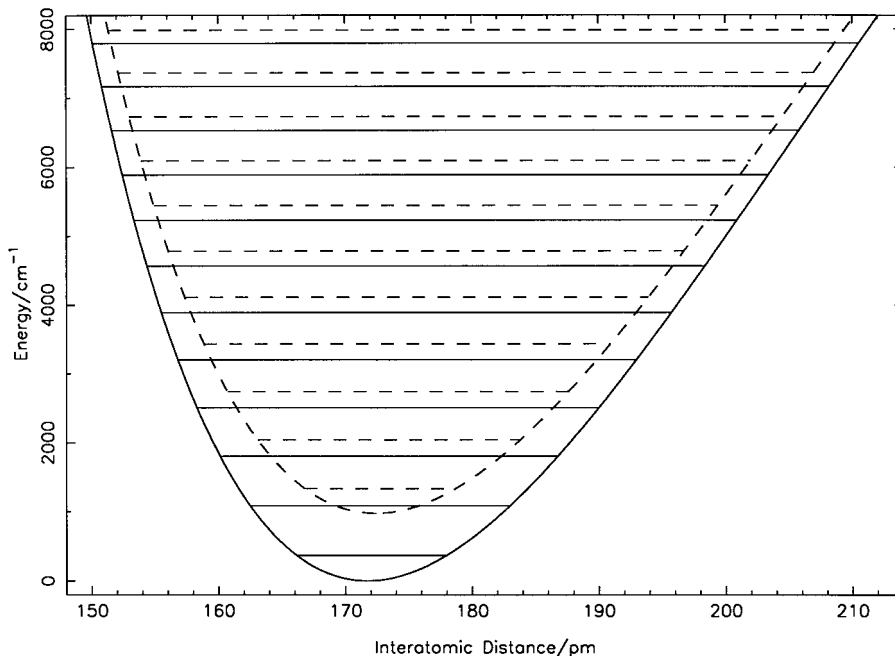


FIG. 4. The interatomic potentials and vibrational levels for the BrO X_1 (solid outer curve) and X_2 states.

X_1 , $v = 1-0$ band (19, 20), and calculated positions of the $J = 1/2-3/2$, $v = 0$ X_2-X_1 fine-structure transitions. In combining the infrared data sets, 0.0009 cm^{-1} was subtracted from the diode-laser measurements of Butler *et al.* (19) to be consistent with the calibration of Orlando *et al.* (20). The fine-structure transitions were used to fix the values of A_0 for the two main isotopes. These line positions were provided by Tamassia and Brown (21) who recently measured the LMR spectrum of the X_1 , $v = 2-0$ band and fitted a merged data set which also included the McKellar LMR data (18) of the fine-structure band, infrared data cited above, and $v = 0, 1$, and 2 rotational data provided by us. The uncertainty of the calculated transitions has been chosen so that our calculated A_0 value has the same uncertainty as that obtained by Tamassia. The vibrational dependence of the spin-orbit coupling constant, A , has a very small effect on the fitted constants and was included in the fit as a series of fixed parameters. The vibrational dependence was determined from the derived potential functions for the two states as described in the next section. Since the potential functions are derived from the fitted parameters, the determination of the vibrational dependence of A involved a short iterative procedure. Data have been weighted inversely as the square of their uncertainties. Calculated uncertainties of the parameters are approximately 1σ .

Although BrO is a very good example of a Hund's case (a) molecule, $A/B \approx -2280$, the Hamiltonian is the effective Hamiltonian which was discussed by Brown *et al.* (25). This is given in Eq. [1a]. The hyperfine Hamiltonian is given in Eq. [1c]:

$$\begin{aligned} \mathcal{H}_v = & T_v + B_v \mathbf{N}^2 - D_v \mathbf{N}^4 + H \mathbf{N}^6 \\ & + (1/2)[(A_v + A_{D,v} \mathbf{N}^2 + A_H \mathbf{N}^4), L_z S_z]_+ \\ & + \gamma \mathbf{N} \cdot \mathbf{S} + (1/4)[(p_v + p_{D,v} \mathbf{N}^2), (\Lambda_+^2 S_- N_- \\ & + \Lambda_-^2 S_+ N_+)]_+ - (q/2)(\Lambda_+^2 N_-^2 + \Lambda_-^2 N_+^2) \end{aligned} \quad [1a]$$

where

$$\begin{aligned} B_v = & \sum_l Y_{l,1}(v + 1/2)^l \\ D_v = & - \sum_l Y_{l,2}(v + 1/2)^l \\ H \approx & Y_{03} \end{aligned} \quad [1b]$$

and

$$\begin{aligned} \mathcal{H}_{\text{hfs}} = & a I_z L_z + b_F \mathbf{I} \cdot \mathbf{S} + c(I_z S_z - \mathbf{I} \cdot \mathbf{S}/3) \\ & + (1/2)d(\Lambda_+^2 I_- S_- + \Lambda_-^2 I_+ S_+) + C \mathbf{I} \cdot \mathbf{N} \\ & + [(e Q q_1 + N_z S_z e Q q_s)(3I_z^2 - \mathbf{I}^2) \\ & + e Q q_2(I_x^2 - I_y^2)]/[4I(2I - 1)]. \end{aligned} \quad [1c]$$

An advantage of this Hamiltonian is that the various parameters have well-defined isotope dependencies. This has allowed fitting the spectra of all four isotopomers, $^{79,81}\text{Br}^{16,18}\text{O}$, with a single set of isotopically invariant parameters. Not shown in

Eq. [1c] are the vibrational dependencies and centrifugal distortion terms. These will be discussed below.

In Eq. [1b] the $Y_{l,n}$ are the Dunham coefficients given by

$$Y_{l,n} = \mu^{-(l+2n)/2} U_{l,n} \left(1 + \frac{m_e \Delta_{l,n}^{\text{O}}}{M_{\text{O}}} + \frac{m_e \Delta_{l,n}^{\text{Br}}}{M_{\text{Br}}} \right), \quad [2]$$

where μ is the reduced mass and $U_{l,n}$ is isotopically invariant. This form has been discussed by Watson (26). The exception to the isotope relation is $Y_{00} \propto \mu^{-1}$.

Because we have determined a number of vibrational and centrifugal distortion terms for some of the constants, we have adopted a notation which we illustrate with the definitions

$$A_v = \sum_{l \geq 0} A_{l,0} \left(v + \frac{1}{2} \right)^l \quad [3a]$$

$$A_{D_v} = \sum_{l \geq 0} A_{l,1} \left(v + \frac{1}{2} \right)^l. \quad [3b]$$

We define the isotope dependencies such that if an operator is multiplied by an expression of the form

$$Z_{l,n} (v + 1/2)^l [N(N + 1)]^n, \quad [4a]$$

then

$$Z_{l,n} \propto r \mu^{-(l+2n)/2}, \quad [4b]$$

where r contains the mass and/or nuclear moment isotope dependence of Z_{00} . These well-defined isotopic relations were fixed within the parameter input file for the program SPFIT (31) and the independent parameters determined using global fits to all isotopic data. All of the fitted parameters are defined relative to $^{79}\text{Br}^{16}\text{O}$ using fixed ratios of the reduced masses, quadrupole moments, and magnetic moments (32, 33). The output file from SPFIT which contains the input data, observed minus calculated frequencies, correlation coefficients, and parameters for all the isotopic species has been deposited with the Journal.

RESULTS AND DISCUSSION

Rotational and Fine-Structure Constants and the Interatomic Potentials

The present study greatly extends the high-resolution observations of $\text{BrO } X^2\Pi_i$ rovibrational states. By including $X_1^2\Pi_{3/2}$ rotational spectra up to $v = 8$, $X_2^2\Pi_{1/2}$ spectra up to $v = 7$, as well as the previously unobserved $^{79,81}\text{Br}^{18}\text{O}$ in both its X_1 and X_2 states in a global fit, we have been able to determine a set of isotopically independent parameters which describe the equilibrium values and the vibrational dependencies of the rotation and Λ -doubling constants. Extension of the observed

spectra to higher J has also resulted in a more precise determination of the centrifugal distortion effects. The fit of all four isotopic species has allowed the first determination of an effective electron spin-rotation constant γ , and also the deviation of the rotational constants from the Born-Oppenheimer approximation. The constants have been defined in the preceding equations and are given in Table 2. Table 2 lists the deviations from the Born-Oppenheimer approximation as contributions to the $^{79}\text{Br}^{16}\text{O}$ rotational constant. From these one obtains $\Delta_{01}^{\text{O}} = -1.9630(39)$ and $\Delta_{01}^{\text{Br}} = -1.124(48)$, which are of the order magnitude expected for these constants (26).

Brown and Watson (34) have shown that the spectroscopic parameters $Y_{l,n}$ and the fine-structure constants $A_{l,n}$ can be used to generate a set of Dunham constants for each state

$$Y_{l,n}^* = Y_{l,n} \pm A_{l,n}/2, \quad [5]$$

where the sum refers to the $X_1^2\Pi_{3/2}$ state and the difference refers to the $X_2^2\Pi_{1/2}$ state. From the $Y_{l,n}^*$ for each state, one can use the Dunham relations to derive the internuclear potential coefficients in the expansion

$$V(\xi) = a_0 \xi^2 \left(1 + \sum_{i \geq 1} a_i \xi^i \right), \quad [6]$$

where $\xi = (r_e - r)/r_e$. The a_i 's can then be used to calculate the $Y_{l,0}^*$ and the vibrational intervals for each state. An accurate knowledge of the vibrational level spacing in each manifold is required to determine the vibrational state dependence of the fine-structure interval in the global fit since the fine-structure constant for each v as given by Eq. [3a] may be represented by

$$\begin{aligned} A_{l,0} &= Y_{l,0}^*(^2\Pi_{3/2}) - Y_{l,0}^*(^2\Pi_{1/2}) \\ A_{00} &= A_e + Y_{00}^*(^2\Pi_{3/2}) - Y_{00}^*(^2\Pi_{1/2}). \end{aligned} \quad [7]$$

Here A_e is the isotopically independent value for the fine-structure interval, and the isotopic dependence of the difference in Y_{00}^* is small compared to experimental uncertainty.

Table 3 shows the Dunham constants, potential coefficients, and molecular constants derived from the fitted parameters. The potentials derived from these constants are plotted in Fig. 4. The difference between these potentials can be interpreted as the variation of A with internuclear distance. A Birge-Sponer plot using the calculated $Y_{l,0}^*$ constants of the X_1 state predicts a dissociation energy D_e of $20\,530 \text{ cm}^{-1}$. Although this number is determined from only the rotational spectra of the ground and lowest eight excited vibrational states, it is in fair agreement with the value of $19\,680 \pm 140 \text{ cm}^{-1}$ determined from studies of the $A-X$ system (9). A similar extrapolation for the X_2 state gives $D_e = 19\,860 \text{ cm}^{-1}$, which is consistent with both states dissociating to the same products.

Note that the bond length in the X_2 state is 0.684 pm longer than in the X_1 state. Y_{10} is 14.934 cm^{-1} lower for $^{79}\text{Br}^{16}\text{O}$ in its

TABLE 2
BrO Molecular Parameters^a

Parameter	Isotopic Ratio	Value in MHz
$Y_{00}^*(^2\Pi_{3/2}) - Y_{00}^*(^2\Pi_{1/2})$	μ^{-1}	118.124
A_{10}	$\mu^{-1/2}$	447 683.800
A_{20}	μ^{-1}	264.796
A_{30}	$\mu^{-3/2}$	-4.702
A_{40}	μ^{-2}	-0.143
$\nu_0(^{79}\text{Br}^{16}\text{O}, X_1 \text{ state})$	N/A	21 687 307.38(110)
$\nu_0(^{81}\text{Br}^{16}\text{O}, X_1 \text{ state})$	N/A	21 642 720.96(108)
U_{01}/μ	μ^{-1}	12 834.9632(45)
$U_{01}\Delta_{01}^{\text{Br}}m_e/(\mu M_{\text{Br}})$	$(M_{\text{Br}}\mu)^{-1}$	-0.1003(43)
$U_{01}\Delta_{01}^{\text{O}}m_e/(\mu M_{\text{O}})$	$(M_{\text{O}}\mu)^{-1}$	-0.86410(170)
Y_{11}	$\mu^{-3/2}$	-109.16430(102)
Y_{21}	μ^{-2}	-0.19916(44)
Y_{31}	$\mu^{-5/2}$	-0.013221(73)
$Y_{41} \times 10^3$	μ^{-3}	-0.3061(53)
Y_{02}	μ^{-2}	-0.01788462(121)
$Y_{12} \times 10^3$	$\mu^{-5/2}$	-0.06602(184)
$Y_{22} \times 10^6$	μ^{-3}	-4.14(74)
$Y_{32} \times 10^6$	$\mu^{-7/2}$	-0.323(74)
$Y_{03} \times 10^6$	μ^{-3}	-0.01011(102)
A_e (average)	1	-29 242 754.2(47)
$\Delta A_e(^{79}\text{Br}^{16}\text{O}-^{81}\text{Br}^{16}\text{O})$	N/A	-13.91(244)
A_{01}	μ^{-1}	102.0377(40)
A_{11}	$\mu^{-3/2}$	1.01746(72)
A_{21}	μ^{-2}	0.020852(200)
$A_{31} \times 10^3$	$\mu^{-5/2}$	0.6490(183)
$A_{02} \times 10^3$	μ^{-2}	0.30982(131)
$A_{12} \times 10^6$	$\mu^{-5/2}$	6.64(78)
γ	μ^{-1}	-670.0(45)
p_{00}	μ^{-1}	1 827.9176(268)
p_{10}	$\mu^{-3/2}$	-13.524(37)
p_{20}	μ^{-2}	-0.3314(100)
$p_{30} \times 10^3$	$\mu^{-5/2}$	-3.31(91)
$p_{01} \times 10^3$	μ^{-2}	-0.1320(280)
$p_{11} \times 10^3$	$\mu^{-5/2}$	-0.2456(244)
q	μ^{-2}	-0.6806(80)
a_{00}	g_N	641.481(134)
a_{10}	$g_N\mu^{-1/2}$	-11.498(256)
b_F	g_N	18.23(95)
c_{00}	g_N	-425.51(157)
c_{10}	$g_N\mu^{-1/2}$	8.36(76)
d_{00}	g_N	849.44(70)
d_{10}	$g_N\mu^{-1/2}$	-15.56(140)
$d_{01} \times 10^3$	$g_N\mu^{-1}$	-3.930(176)
C_I	$g_N\mu^{-1}$	0.06780(64)
eQq_2	Q	862.48(47)
eQq_{100}	Q	658.676(83)
eQq_S	Q	-21.817(87)
eQq_{110}	$Q\mu^{-1/2}$	4.348(111)
$eQq_{101} \times 10^3$	$Q\mu^{-1}$	1.693(247)

^a Except as noted, the parameters are for $^{79}\text{Br}^{16}\text{O}$. The parameters for the other isotopic species are determined using fixed mass (32) and/or nuclear moment ratios (33). Parameters with N/A in the ratio column were determined without using fixed ratios. The first five parameters were calculated from the interatomic potential and were fixed during the fit.

TABLE 3
Potential Constants and Derived Parameters

Parameter	$X_1 \ ^2\Pi_{3/2}$	$X_2 \ ^2\Pi_{1/2}$
a_0/cm^{-1}	312 401.2	302 192.6
a_1	-3.39619	-3.40732
a_2	7.20696	7.23028
a_3	-13.48403	-13.52677
a_4	23.84235	24.57892
a_5	-53.05816	-60.43129
a_6	109.37615	168.49443
Y_{00}^*/cm^{-1}	0.07716	0.07322
Y_{10}^*/cm^{-1}	732.88319	717.94966
Y_{20}^*/cm^{-1}	-4.64905	-4.65785
Y_{30}^*/cm^{-1}	-0.00769	-0.00754
Y_{40}^*/cm^{-1}	-0.00058	-0.00058
r_e/pm	171.7249	172.4089

X_2 state and the difference in ω_0 is calculated to be 14.951 cm^{-1} . A similar calculation based on only the rotational spectra of ClO (35) gives 3.319 cm^{-1} , which compares favorably to the experimental value of 3.277 cm^{-1} (36). Comparable agreement is expected for BrO. Table 4 compares derived vibrational intervals with observed values. The agreement is quite good. The vibrational contributions to the values of A_0 are 7.4727 and 7.4511 cm^{-1} for $^{79}\text{Br}^{16}\text{O}$ and $^{81}\text{Br}^{16}\text{O}$, respectively. Were A_e entirely isotope independent, the magnitude of the measured fine-structure interval of $^{81}\text{Br}^{16}\text{O}$ would be 466.9 MHz larger than that of $^{79}\text{Br}^{16}\text{O}$. The actual difference is 453.0 MHz . In comparing the A values reported in this work with others in the literature, it should be noted that the values reported here do not include any contribution from γ . The values of A previously reported differ from the ones reported here by γ , which contributes a small isotope dependence. Thus, the magnitude of the effective A_e of $^{81}\text{Br}^{16}\text{O}$ is $\approx 13.9(24) \text{ MHz}$ less than that of $^{79}\text{Br}^{16}\text{O}$. This is about the same size as the isotopic dependence of the fine-structure constant in atomic Br but of opposite sign.

There are two measurements of the fine-structure transitions of atomic Br near 3684 cm^{-1} with the ^{81}Br transitions higher by $13.6_{-2}^{+5} \text{ MHz}$ (37) and $11.7(30) \text{ MHz}$ (38). Because the effective A in the molecule includes higher order terms which have no direct counterpart in the atom and because the residual

TABLE 4
Derived Vibrational Intervals for $^{79}\text{Br}^{16}\text{O}$

$v' - v''$	$X_1 \ ^2\Pi_{3/2}$		$X_2 \ ^2\Pi_{1/2}$
	Derived	Observed	Derived
1 - 0	723.557(30)	723.4107 ^a	708.607(35)
2 - 0	1437.730(60)	1437.4721 ^b	1407.813(70)

^a This work using data from Refs. (19, 20).

^b From Ref. (21).

isotope effect has an experimental uncertainty which is significant compared to its magnitude, the agreement of the calculated and observed isotope shifts is quite satisfactory. The remainder is very small compared to the magnitude of A_e and is comparable to deviations from the Born–Oppenheimer approximation, i.e., $|A_e m_e (M_{79}^{-1} - M_{81}^{-1})| \approx 5$ MHz. At the level of theory employed here, it is difficult to be certain that all contributions of this magnitude are properly accounted for. Any further interpretation of this effect is beyond the scope of the present paper.

The spin–rotation constant, γ , obtained directly from the fit represents an effective parameter that has been defined by Brown *et al.* (25). The present analysis assumes that γ varies as μ^{-1} . The contribution of γ to each energy level is most readily described by considering the off-diagonal term $\langle {}^2\Pi_{3/2}, v | \mathcal{H} | {}^2\Pi_{1/2}, v \rangle$ in a Hund's case (a) basis. This matrix element contains a term which is often written as $(B - \gamma/2)[(J + \frac{3}{2})(J - \frac{1}{2})]^{1/2}$. The net result is that the fitting parameter γ absorbs the contributions from all terms which vary as μ^{-1} and make the term $B - \gamma/2$ different from B . Therefore, the value of $\gamma = 670.4(4.5)$ MHz should be interpreted cautiously. It is a rather large parameter, but its effects on the observed spectrum are subtle. For a case (a) molecule, the apparent difference in rotational constants of the X_1 and X_2 components of a ${}^2\Pi$ state is approximately

$$B(X_1) - B(X_2) = A_D + 2(B - \gamma/2)^2/(A - 2B). \quad [8]$$

The difference in the isotopic shift in this quantity as compared to one calculated with $\gamma = 0$ is approximated by

$$\frac{2\gamma B}{A - 2B} (\rho - \rho^2), \quad [9]$$

where ρ is the ratio of the reduced mass of the reference species to that of the isotopically substituted species. With respect to ${}^{79}\text{Br}^{16}\text{O}$, this contribution is almost 50 kHz for ${}^{18}\text{O}$ substitution and 2.5 kHz for ${}^{81}\text{Br}$ substitution. Although both these values give easily measurable frequency shifts in the submillimeter region, and although the value of γ derived from ${}^{81}\text{Br}$ substitution alone is quite close to that derived from all four species, the change in rotational constant is small and may be contaminated by effects not considered in the model Hamiltonian. Vibrational and centrifugal distortion corrections to γ have not been included in the fit. Those corrections are poorly determined, do not improve the quality of the fit, and can be absorbed in the effective values of the $A_{l,1}$. The constant γ_{10} , by analogy with similar constants, is expected to be $\approx 1\%$ of the magnitude of γ . Neglect of a constant of this size will not change the values of the $A_{l,1}$ enough to significantly affect the $Y_{l,n}^*$ calculated in Eq. [5] or the potentials derived from them.

The fact that the vibrational wavefunctions for the X_1 and X_2 states are slightly displaced from each other contributes to the

value of γ by an amount that is larger than the calculated uncertainty in γ . This is not incorporated into the fit, but the influence of imperfect spatial overlap on the calculated value of γ can be estimated. The quantity

$$S_{v,v} = \langle \Omega = 3/2, v | \Omega = 1/2, v \rangle \quad [10]$$

may be calculated from the Dunham potentials described above. For $v = 0$, $S_{0,0} = 0.99657$. The actual quantity determined is then

$$\gamma = S_{0,0}\gamma^* + 2B(1 - S_{0,0}), \quad [11]$$

where γ^* is the constant for the hypothetical $S_{0,0} \equiv 1$. The second term on the right-hand side of Eq. [11] contributes 92.2 MHz and decreases the magnitude of the effective γ derived from the fit by about that amount.

The Λ -doubling constants p and q as well as γ are often used to deduce information on the excited states of diatomic molecules. To second order, the expressions for these constants are

$$p = -2 \sum_i \pm \frac{\langle {}^2\Pi | L_+ A | {}^2\Sigma^\pm \rangle \langle {}^2\Sigma^\pm | L_- B | {}^2\Pi \rangle}{\Delta E_i}, \quad [12]$$

$$q = -2 \sum_i \pm \frac{\langle {}^2\Pi | L_+ B | {}^2\Sigma^\pm \rangle^2}{\Delta E_i}, \quad [13]$$

and

$$\gamma = \gamma^{(1)} + \gamma^{(2)}, \quad [14]$$

where $\gamma^{(2)}$ is the dominant term and is given by

$$\gamma^{(2)} = \sum_i \frac{\langle {}^2\Pi | L_+ A | {}^2\Sigma^\pm \rangle \langle {}^2\Sigma^\pm | L_- B | {}^2\Pi \rangle}{\Delta E_i}. \quad [15]$$

Equations [12] and [13] imply that $p/q \approx A/B$. For ${}^{79}\text{Br}^{16}\text{O}$, $p_{00}/q = -2686(32)$ and $A_e/Y_{01} = -2278$, which suggests that the single perturber approximation is fairly good for the $X^2\Pi_i$ state. The positive value of p obtained from the fit implies that Σ^+ states dominate the sum in Eq. [12]. It also implies that $\gamma \approx -p/2$. For ${}^{79}\text{Br}^{16}\text{O}$, $p/2 = 913.96$ MHz, $\gamma = -670.5$ MHz, and $\gamma^* = -762$ MHz. Considering the small magnitude of the effect from which γ is derived, this is reasonable agreement. The fact that the effects of Σ^+ and Σ^- states cancel in the expression for p , but add for γ , is further indication of one primary perturbing state. If only one ${}^2\Sigma^+$ state is responsible for most of the perturbation, then it is near $27\,500\text{ cm}^{-1}$, very close to the $A^2\Pi_i$ state (6–9). Amano (39) performed a similar calculation for ClO and estimated that the ${}^2\Sigma^+$ state was almost coincident with the $A^2\Pi_i$ in that mole-

cule. Both molecules show predissociation of the $A^2\Pi_i$ state due to the presence of as yet unobserved states. In the case of ClO, Lane *et al.* (40) have reported calculations which show the presence of numerous repulsive states, including several $^2\Sigma$ states near the $A^2\Pi_i$ state. Recently Li *et al.* (41) have carried out a theoretical study of the low-lying excited states of BrO and also find repulsive $^2\Sigma^+$ and $^2\Sigma^-$ states crossing the $A^2\Pi_i$ state.

Hyperfine Constants

The magnetic hyperfine constants determined in this study are more complete and more precise than those previously determined. The main terms have been shown in Eq. [1c]. In addition, linear vibrational dependencies of a , d , and c are included in the fit. These have been given in Table 2. No vibrational dependence was included for the small and less well-determined constants C_l and b_F , although we note that the vibrational dependence of b_F cannot be separated from that of c . The nonaxial component of the nuclear spin-rotation constant C_l is too highly correlated with other constants to be reliably determined and was excluded from the fit. Centrifugal distortion of d is required to fit the spectrum. The centrifugal distortions of the other primary magnetic constants cannot be reliably determined since they are strongly correlated with C_l and b_F and cannot be decorrelated by their isotope effects. This results in small contributions to the effective values of C_l and b_F . C_l is the average of the effective nuclear spin-rotation constants for the X_1 and X_2 states. It contains a contribution from the centrifugal distortion of a which may lower the value of the effective C_l by several kilohertz. This is considerably smaller than C_l and does not affect its interpretation. Although all the parameters reported in Table 2 are determined in a global fit, it is useful to think of b_F as derived from the difference in effective nuclear spin-rotation constants for the two states. This is given to second order by

$$C_l(X_1) - C_l(X_2) = \frac{2\left(B - \frac{\gamma}{2}\right)\left(b_F - \frac{c}{3}\right)}{E(X_2) - E(X_1)} \quad [16]$$

or about 144 kHz. This may contain contributions of a few kilohertz from centrifugal distortion on the quantity $(b_F + 2c/3)$ as well as small differences in C_l resulting from differences in the mixing of each X state with other electronic states. Each kilohertz of change in the LHS of Eq. [16] contributes about 2 MHz to the effective value of b_F .

The quadrupole coupling constants include a term which is in effect the difference between the X_1 and X_2 state quadrupole coupling constants. These are fitted as the average eQq_1 and difference eQq_s . Linear vibrational dependence and centrifugal distortion on the average value are included in the fit. The nonaxial quadrupole constant eQq_2 contributes to the splitting of the Λ -doublets. Although eQq_2 is large, its contribution is

on the order of the Λ -doubling on the X_2 state (17) and is largest for the weak $\Delta F = 0$ transitions. Its largest contributions to splittings observed in this work are about 3 MHz. The quadrupole constants are also given in Table 2.

Using the definitions of the magnetic hyperfine and quadrupole coupling constants

$$\begin{aligned} a &= 2g_N\beta\beta_N\langle 1/r^3 \rangle_L \\ b_F &= (8\pi/3)g_e g_N\beta\beta_N\langle \psi^2(0) \rangle_S \\ c &= (3/2)g_e g_N\beta\beta_N\langle (3\cos^2\theta - 1)/r^3 \rangle_S \\ d &= (3/2)g_e g_N\beta\beta_N\langle \sin^2\theta/r^3 \rangle_S \\ eQq_1 &= eQ\langle (3\cos^2\theta - 1)/r^3 \rangle_T \\ eQq_2 &= -3eQ\langle \sin^2\theta/r^3 \rangle_T, \end{aligned} \quad [17]$$

it is possible to determine the electron distribution in the molecule. In Eq. [17] L refers to the electrons responsible for the orbital angular momentum, S to those responsible for the spin, and T to all the electrons. It is important to remember, however, that Eq. [17] defines the hyperfine constants in terms of a single average Π state. There is an implicit assumption that these constants have identical values for both the X_1 and X_2 states. Although this assumption probably becomes less valid as the spin-orbit coupling increases, it is not possible to determine changes in the individual magnetic constants experimentally. Thus, the a reported here is actually

$$a = \frac{(\langle X_1|h_+|X_1 \rangle + \langle X_2|h_-|X_2 \rangle)}{2}, \quad [18]$$

where $h_{\pm} = a \pm (b_F + 2c/3)/2$. Similarly, b_F and c are determined from the same expectation values of h_{\pm} as well as $\langle X_1|b_F - c/3|X_2 \rangle$. The magnetic constant d produces significant effects only in the X_2 state. Changes in quadrupole coupling can be determined and seem to indicate that changes in the magnetic hyperfine constants will not seriously affect their interpretation in terms of average constants. Meerts and Dymannus (42) in a study of the Λ -doubling spectrum of NO derive expressions for some of these differences.

Table 5 compares the molecular expectation values $\langle 1/r^3 \rangle_L$ derived from a and $\langle 1/r^3 \rangle_S$ derived from $d + c/3$ with those determined by the relativistic restricted Hartree-Fock calculations of Lindgren and Rosén for atomic Br (43) as well as those of Pyykkö and Wiesenfeld (44). Note that if one uses the appropriate atomic values for $\langle 1/r^3 \rangle_L$ and $\langle 1/r^3 \rangle_S$ to determine the unpaired electron density on the Br atom, the resulting densities are very nearly equal to each other. This is in contrast to the carbon monohalides for which the unpaired electron density derived from the dipolar interaction is slightly lower than that derived from the interaction of the magnetic field induced by the electron orbital motion (45-47). For CBr (47) the derived densities are approximately 17 and 22% when

TABLE 5

Parameters Derived from the Magnetic Hyperfine Constants^a

	BrO	Br Atom ^b	ρ^b	Br Atom ^c	ρ^c
$\langle r^{-3} \rangle_S$	35.60	97.9	36.4	98.7	36.0
$\langle r^{-3} \rangle_L$	32.31	86.5	37.4	87.3	37.0
$\langle \psi(0)^2 \rangle$	0.109	-0.5		-0.5	
$\langle \sin^2 \theta \rangle$	0.8003				

^a r^{-3} and $\psi^2(0)$ in $\text{m}^3 \times 10^{-30}$. Unpaired electron density, ρ_1 in %.

^b Using calculated atomic values from Ref. (43).

^c Using calculated atomic values from Ref. (44).

derived from the dipolar and orbital terms, respectively. Also of interest is the negative contact term predicted by the relativistic calculation. In the absence of other effects, the unpaired p electron should contribute about -39 MHz to b_F . NBr (48), for which the determination of the Fermi contact term is more direct, has $b_F = -10.97(52)$ MHz for N^{79}Br . The positive value of b_F determined for ^{79}BrO , 18.23(95) MHz, may be due to a very small amount (0.2%) of s -orbital character, but interpretation of effects of this size without a high-level relativistic *ab initio* calculation is speculative. For a pure p electron $\langle \sin^2 \theta \rangle = 0.8$ and $c = -d/2$. Within experimental uncertainty, this condition is satisfied for BrO.

The nonaxial quadrupole coupling constant eQq_2 results from a noncylindrical distribution of electron density about the molecular axis. If one assumes that the unpaired electron is entirely responsible for the asymmetry, eQq_2 may be calculated from the fact that the $p(\pi^*)$ orbitals have a single vacancy of which 37% is on the bromine atom. This leads to a calculated value of $eQq_2 = 854$ MHz, which is very close to the experimental value of 862.5(47) MHz. Lindgren and Rosén (43) and Pyykkö and Seth (49) have pointed out that the radial integrals in the hyperfine constants shown in Eq. [17] are not identical. However, the effects are not large enough for Br to affect the conclusion that approximately the same unpaired electron density can be derived from each of the coupling constants that depend upon it.

The change in quadrupole coupling with electronic state may be attributable to several causes. As the spin-orbit coupling becomes larger, the $\Omega = \frac{1}{2}$ and $\frac{3}{2}$ states may mix with other states of the same Ω . For a very large spin-orbit coupling constant, a Hund's case (c) results in which Λ and Σ are not well defined and only Ω is used to identify the states. It is understandable then, that the quadrupole couplings for the two states should be different. Although BrO is best thought of as a case (a) molecule, the contributions of case (c) type behavior to the hyperfine constants should be considered, but quantitative evaluation of these effects is difficult and has not been undertaken here.

A potentially important difference in quadrupole coupling between the X_1 and X_2 states comes from a relativistic contribution. The electric field gradient at the nucleus due to a p

electron is a function of two radial integrals. Fairly general discussions and earlier references may be found in Refs. (43, 49). Pyykkö and Seth (49) recently reported relativistic correction factors which are the ratios of the results of relativistic calculations of $\langle r^{-3} \rangle$ to those of nonrelativistic calculations. For a halogen atom, the coupling constant eQq_{n10} is obtained from the $^2P_{3/2}$ ground state and may be written

$$eQq_{n10} = C_{++}eQq_{n10\text{NR}}, \quad [19]$$

where NR refers to the nonrelativistic value and C_{++} is the correction factor for a $p_{3/2}$ electron. In the molecule the coupling constant for a $p(\pi_{3/2})$ electron in the halogen is

$$eQq(3/2) = \frac{-C_{++}eQq_{n10\text{NR}}}{2} \quad [20]$$

and for $p(\pi_{1/2})$

$$eQq(1/2) = \frac{(C_{++} - 4C_{+-})eQq_{n10\text{NR}}}{6}. \quad [21]$$

If the two states have no other differences, and with an unpaired electron density ρ_s on the halogen, we obtain

$$\Delta(\text{Rel}) = \frac{2\rho_s(C_+ - C_{++})(eQq_{n10})}{3C_{++}}. \quad [22]$$

For light nuclei, $C_{+-} \approx C_{++} \approx 1$, and the difference is small. For a heavy nucleus, this difference is significant. In addition there is a change in interatomic distance between the X_1 and X_2 states which may also influence electron distribution and the field gradient. For the range of vibrational states that have been observed, this change is almost linear with rotational constant. Therefore, the contribution to the change in quadrupole coupling due to structural changes has been estimated by

$$\Delta(\text{Struc}) = eQq_{110} \frac{A_{01}}{Y_{11}}. \quad [23]$$

Table 6 compares the estimated and observed changes in eQq_1 . It is quite large compared with the vibrational change. It amounts to a 3.35% change from X_1 value which may be compared with 0.43% for ClO and 10.5% for IO (24).

Thus, the relativistic and structural effects together do not entirely account for the change in quadrupole coupling. This suggests that differences in electronic structure may affect the magnetic hyperfine parameters as well, but that these differences are probably relatively small compared to the magnitudes of the constants with the exception of b_F . It has already been mentioned that the definitions of the magnetic constants which were employed in the derivation of unpaired electron

TABLE 6
Calculated and Observed eQq_1 Differences/MHz for the Halogen Oxides

Molecule	eQq_{n10}	C_{+-} ^a	C_{++} ^a	ρ_s	$\Delta(\text{Rel})$ ^b	$\Delta(\text{Struc})$ ^c	Total	eQq_s
ClO ^d	109.74	1.01459	1.00323	0.353	0.32	0.09	0.41	0.37(9)
BrO	-769.76	1.08326	1.02831	0.370	-10.1	-4.0	-14.1	-21.82(9)
IO ^e	2292.71	1.23463	1.08604	0.389	81.4	38.5	119.1	198.14(65)

^a From Ref. (49).

^b From Eq. [22].

^c From Eq. [23].

^d From Ref. (35).

^e From Ref. (24).

density are not strictly correct. Nevertheless, the derived unpaired electron densities are consistent irrespective of the constant used in the derivation. Moreover, the derived angular distribution is what is expected from a p electron on the Br atom.

Sakamaki *et al.* (48) have already discussed eQq_1 for BrO in the context of their work on NBr. Although the average value for eQq_1 is about 10 MHz higher than the X_1 value which was available at the time, the validity of their comments is unaffected.

The vibrational changes of the hyperfine constants are consistent with the unpaired electron density gradually moving to oxygen atom and the single bond becoming less ionic as the atoms separate.

CONCLUSION

A set of isotopically independent parameters has been determined which describes the rotational spectrum of BrO to $v = 8$ for the X_1 state and $v = 7$ for the X_2 state. The electron spin-rotation constant and the deviation of the rotational constant from the Born-Oppenheimer approximation have been determined. Interatomic potentials have been derived which allow one to calculate the bond lengths and vibrational frequencies for the two states. The difference in the potential functions has also been interpreted as the variation in fine-structure interval with internuclear distance. The hyperfine constants have been compared with atomic values derived from relativistic calculations to provide information on the electron distribution in the molecule. Interpretation of the hyperfine constants in terms of those of an average Π state gives internally consistent results.

ACKNOWLEDGMENTS

The authors thank F. Tamassia and J. M. Brown for communicating their results prior to publication. They also acknowledge some very useful comments by P. Pyykkö. This paper presents research carried out at the Jet Propulsion Laboratory, California Institute of Technology, under contract with the National Aeronautics and Space Administration.

REFERENCES

1. R. P. Wayne, G. Poulet, P. Biggs, J. P. Burrows, R. A. Cox, P. J. Crutzen, G. D. Hayman, M. E. Jenkin, G. Lebras, G. K. Moortgat, U. Platt, and R. N. Schindler, *Atmos. Environ.* **29**, 2677-2881 (1995).
2. M. A. Workman and J. S. Francisco, *Chem. Phys. Lett.* **293**, 65-71 (1998).
3. M. Alcamí and I. L. Cooper, *J. Chem. Phys.* **108**, 9414-9424 (1998).
4. W. M. Vaidya, *Proc. Ind. Acad. Sci. A* **7**, 321-326 (1938).
5. E. H. Coleman and A. G. Gaydon, *Discuss. Faraday Soc.* **2**, 166-169 (1947).
6. R. A. Durie and D. A. Ramsay, *Can. J. Phys.* **36**, 35-53 (1958).
7. M. Barnett, E. A. Cohen, and D. A. Ramsay, *Can. J. Phys.* **59**, 1908-1916 (1981).
8. A. Loewenschuss, J. C. Miller, and L. Andrews, *J. Mol. Spectrosc.* **81**, 351-362 (1980).
9. D. M. Wilmouth, T. F. Hanisco, N. M. Donahue, and J. G. Anderson, *J. Phys. Chem. A* **103**, 8935-8945 (1999).
10. M. D. Wheeler, S. M. Newman, T. Ishiwata, M. Kawasaki, and A. J. Orr-Ewing, *Chem. Phys. Lett.* **285**, 346-351 (1998).
11. A. Carrington, D. H. Levy, and T. Miller, *J. Chem. Phys.* **47**, 3801-3809 (1967).
12. A. Carrington, P. N. Dyer, and D. H. Levy, *J. Chem. Phys.* **52**, 309-314 (1970).
13. C. R. Byfleet, A. Carrington, and D. K. Russell, *Mol. Phys.* **20**, 271-278 (1971).
14. J. M. Brown, C. R. Byfleet, B. J. Howard, and D. K. Russell, *Mol. Phys.* **23**, 457-468 (1972).
15. F. X. Powell and D. R. Johnson, *J. Chem. Phys.* **50**, 4596 (1969).
16. T. Amano, A. Yoshinaga, and E. Hirota, *J. Mol. Spectrosc.* **44**, 594-598 (1972).
17. E. A. Cohen, H. M. Pickett, and M. Geller, *J. Mol. Spectrosc.* **87**, 459-470 (1981).
18. A. R. W. McKellar, *J. Mol. Spectrosc.* **86**, 43-54 (1981).
19. J. E. Butler, K. Kawaguchi, and E. Hirota, *J. Mol. Spectrosc.* **104**, 372-379 (1984).
20. J. J. Orlando, J. B. Burkholder, A. M. R. P. Bopegedera, and C. J. Howard, *J. Mol. Spectrosc.* **145**, 278-289 (1991).
21. F. Tamassia and J. M. Brown, International Symposium on Molecular Spectroscopy. Abstract WG06, Columbus, Ohio, 1997, and personal communication.
22. M. K. Gilles, M. L. Polak, and W. C. Lineberger, *J. Chem. Phys.* **96**, 8012-8020 (1992).
23. M. W. Chase, Jr., *J. Phys. Chem. Ref. Data* **25**, 1069-1111 (1996).
24. C. E. Miller, and E. A. Cohen, International Symposium on Molecular Spectroscopy. Abstract TJ06, Columbus, Ohio, 1999.

25. J. M. Brown, E. A. Colbourn, J. K. G. Watson, and F. D. Wayne, *J. Mol. Spectrosc.* **74**, 294–318 (1979).
26. J. K. G. Watson, *J. Mol. Spectrosc.* **45**, 99–113 (1973).
27. H. M. Pickett, R. L. Poynter, E. A. Cohen, M. L. Delitsky, J. C. Pearson, and H. S. P. Müller, *J. Quant. Spectrosc. Radiat. Transfer* **60**, 883–890 (1998).
28. M. Birk, R. R. Friedl, E. A. Cohen, H. M. Pickett, and S. P. Sander, *J. Chem. Phys.* **91**, 6588–6597 (1989).
29. R. R. Friedl, M. Birk, J. J. Oh, and E. A. Cohen, *J. Mol. Spectrosc.* **170**, 383–396 (1995).
30. H. S. P. Müller, C. E. Miller, and E. A. Cohen, *J. Chem. Phys.* **107**, 8292–8302 (1997).
31. H. M. Pickett, *J. Mol. Spectrosc.* **148**, 371–377 (1991).
32. G. Audi and A. H. Wapstra, *Nucl. Phys. A* **595**, 409–480 (1995).
33. H. H. Brown and J. G. King, *Phys. Rev.* **142**, 53–59 (1966).
34. J. M. Brown and J. K. G. Watson, *J. Mol. Spectrosc.* **65**, 65–74 (1977).
35. B. J. Drouin, C. E. Miller, and E. A. Cohen, unpublished manuscript.
36. J. B. Burkholder, P. D. Hammer, C. J. Howard, A. G. Maki, G. Thompson, and C. Chackerian, *J. Mol. Spectrosc.* **124**, 139–161 (1987).
37. J. V. V. Kasper, C. R. Pollock, R. F. Curl, Jr., and F. K. Tittel, *Chem. Phys. Lett.* **77**, 211–213 (1981).
38. D. D. Nelson, Jr., A. Schiffman, K. R. Lykke, and D. J. Nesbitt, *Chem. Phys. Lett.* **153**, 105–111 (1988).
39. T. Amano, E. Hirota, and Y. Morino, *J. Mol. Spectrosc.* **27**, 257–265 (1968).
40. I. C. Lane, W. H. Howie, and A. J. Orr-Ewing, *Phys. Chem. Chem. Phys.* **1**, 3087–3096 (1999).
41. Y. Li, J. S. Francisco, and K. A. Peterson, *J. Chem. Phys.*, in press.
42. W. L. Meerts and A. Dymanus, *J. Mol. Spectrosc.* **44**, 320–346 (1972).
43. I. Lindgren and A. Rosén, *Case Stud. At. Phys.* **4**, 93–196, 197–298 (1974).
44. P. Pyykkö and L. Wiesenfeld, *Mol. Phys.* **43**, 557–580 (1981).
45. S. Saito, Y. Endo, M. Takami, and E. Hirota, *J. Chem. Phys.* **78**, 116–120 (1983).
46. Y. Endo, S. Saito, and E. Hirota, *J. Mol. Spectrosc.* **94**, 199–207 (1982).
47. M. Hassouna, A. Walters, C. Demuyck, and M. Bogey, *J. Mol. Spectrosc.* **200**, 16–24 (2000).
48. T. Sakamaki, T. Okabayashi, and M. Tanimoto, *J. Chem. Phys.* **109**, 7169–7175 (1998).
49. P. Pyykkö and M. Seth, *Theor. Chem. Acc.* **96**, 92–104 (1997).